Soft Matter

View Online
Dynamic Article Links

Cite this: *Soft Matter*, 2011, **7**, 8628

www.rsc.org/softmatter

PAPER

Slip boundary conditions based on molecular kinetic theory: The critical shear stress and the energy dissipation at the liquid–solid interface

Feng-Chao Wang and Ya-Pu Zhao*

Received 29th March 2011, Accepted 13th June 2011
DOI: 10.1039/c1sm05543g

The boundary slip and its mechanism were investigated using theoretical analysis and molecular dynamic simulations. We proposed a new slip boundary condition based on molecular kinetic theory, which was extended by the introduction of the critical shear stress, which determines the onset of the slip, and the energy dissipation near the liquid–solid interface at high shear stress. Our results revealed that the critical shear stress increases exponentially with the liquid–solid interactions. In particular, we discussed the energy dissipation contributed from the friction between the liquid layers near the interface. The results demonstrated that the momentum transfer among the liquid layers and the bulk liquid must be considered according to the wetting conditions of the solid surface, which can interpret the contradictory published results of slip behavior at high shear stress. The analytical expression of our slip boundary condition can be compared with the simulation results since it uses parameters consistent with that used in our molecular dynamic simulations. Furthermore, we suggested a dimensionless number to qualify the transition from Poiseuille-like to plug-like flow in the carbon nanotubes. These findings can enhance our understanding of the boundary slip.

1. Introduction

There is a long-standing and historic controversy in the community of fluid mechanics, running for over 180 years, on the slip boundary condition (SBC) and its mechanism.[1] For macroscopic flows, the no-slip boundary condition, which means that the relative liquid–solid velocity is assumed to be zero, is widely adopted since it can reproduce the velocity profiles measured in experiments.[2,3] However, this assumption is debated, especially for cases on a microscopic scale. Recent controlled experiments[4–10] and molecular dynamic (MD) simulations[11–16] have demonstrated an apparent motion of liquid relative to the solid surface, which indicates the breakdown of the no-slip boundary condition. Consequently, the SBC must be considered.

The study of the SBC can be traced back to Navier, whose pioneering work in 1823 proposed a linear SBC $V_s = L_s\dot{\gamma}$, in which L_s is the slip length with a constant value and $\dot{\gamma}$ denotes the shear rate.[17] According to Brillouin's expression of the shear stress at the liquid–solid interface $\tau = kV_s$, where k is the friction coefficient, and the slip length can be defined as $L_s = V_s/\dot{\gamma} = \eta/k$.[18] Slip at the liquid–solid interfaces becomes significant when referring to the micro- and nano-scale flow, which is of fundamental physical interest and has a broad range of practical applications in many areas,[19] from designing nanofluidic devices[20,21] to understanding the biological ionic channels.[22]

Over the past several decades, reassessment of the SBC has received considerable attention.[2–16,23–25] Despite the aforementioned notable progress, there are still some unclear and controversial aspects of the boundary slip, that are yet to be adequately resolved. First, there is some debate on the transition from the no-slip to slip regime. As Brillouin's expression indicates, slip occurs once the shear stress is applied, though the slip velocity or the slip length might be too small to be discerned. Alternatively, experimental investigations on thin-film drainage using surface force apparatus observed that slip occurs only when the driving force exceeds a critical value, which is defined as the critical shear stress, τ_c. Thus the shear stress can be written as $\tau = \tau_c + \eta V_s/L_s$.[26] Comparing these two descriptions, one can find that the choice of model is essential in determining the slip length.[27] Second, shear-dependent slip was reported in some experiments,[6,7] in which the measured slip length is a non-linear function of the shear rate. However, there has been no consensus so far. More recent experiments using a different method observed that the slip length is independent of shear rate within the range of experimentally accessible shear rates and attributed the contradiction to the experimental methods, as well as the measuring accuracy.[9,10] On the other hand, the shear rate used in MD studies is always extremely high compared with experiments due to the small dimensions of the channel. Thus, MD simulations were extensively used to investigate the shear-dependent slip behavior.[11–15] The controversial published results of MD simulations at such a high shear rate indicated that momentum transfer between the liquid and the solid should be examined carefully.[14] Third, MD results observed both Poiseuille-like and

State Key Laboratory of Nonlinear Mechanics, Institute of Mechanics, Chinese Academy of Sciences, Beijing, 100190, People's Republic of China. E-mail: yzhao@imech.ac.cn

plug-like flow in the carbon nanotube (CNT).[28–30] The Poiseuille-like flow, which corresponds to the prediction of the continuum theory, is easily understood. If the slip length is extremely large compared with the width scale of the channel, the velocity profiles seems to be plug-like. Additionally, several indications, however, suggest another type of plug-like flow. The velocity profiles cannot be simply fitted with a parabola, which looks like a near-flat parabolic or is even truly flat. This type of plug-like flow is analogous to the electro-osmotic flow, in which the velocity results from the balance between the electric driving force in the Debye layer and the viscous force at the solid surface.[23] It is imperative to explore the influence of the driven force and the viscous force on the flow velocity profiles in the CNT. Though MD simulations can provide insight into the fluid transport at the nanoscale, the computational results should be well represented by a theoretical model. As far as we are aware, there are only a few existing literature reports on such theoretical approaches of SBC combined with the MD parameters.[12,14–16]

The primary goal of this work is to propose a new SBC and to answer the three questions mentioned above. Our SBC, which is based on molecular kinetic theory (MKT),[31] was extended by the introduction of the critical shear stress and the energy dissipation near the liquid–solid interface. Besides, the analytical expression of our SBC can be compared with the MD results since it uses parameters consistent with the ones used in our MD simulations. Our SBC characterizes the slip behavior over a large range of shear stress, which can be divided into three regimes: (i) No-slip regime. The boundary slip would not occur unless the critical shear stress is reached. Microscopic explanation on this issue associated with the energy corrugation of the solid surface is presented in this work. The dependence of the critical shear stress on the liquid–solid interaction is discussed theoretically and compared with MD results. (ii) Navier slip regime. If the shear stress is larger than τ_c and yet not very high, the boundary slip occurs with a constant slip length. In this regime, our SBC can be reduced to Navier's SBC. (iii) Shear-dependent slip regime. The slip length increases with the shear rate. The shear-dependent boundary slip at even higher shear stress exhibits two different kinds of nonlinear responses according to the wetting conditions of the solid surface. A dissipation factor is introduced into the MKT model to take account of the energy dissipation due to the relative sliding between the individual liquid layers near the interface. The transition from Poiseuille-like to plug-like flow in the CNT is sketched by a suggested nondimensional number. This new SBC can be not only compared with other slip models, but also verified in our MD simulations under various situations, by varying the driven force exerted on the liquid and the liquid–solid interactions.

2. Simulation details

MD simulations were performed to investigate the slip behavior in the CNT, as shown in Fig. 1(a, b). We simulated a force driven flow in an armchair CNT with a diameter of 8.69 nm and a length of 14.76 nm. The CNT was modeled as a rigid channel since it has been proved that this procedure results in limited variation of the flow velocity compared with the flexible CNT walls.[16,29] In order to perceive the physical essence, the liquid in our simulations was

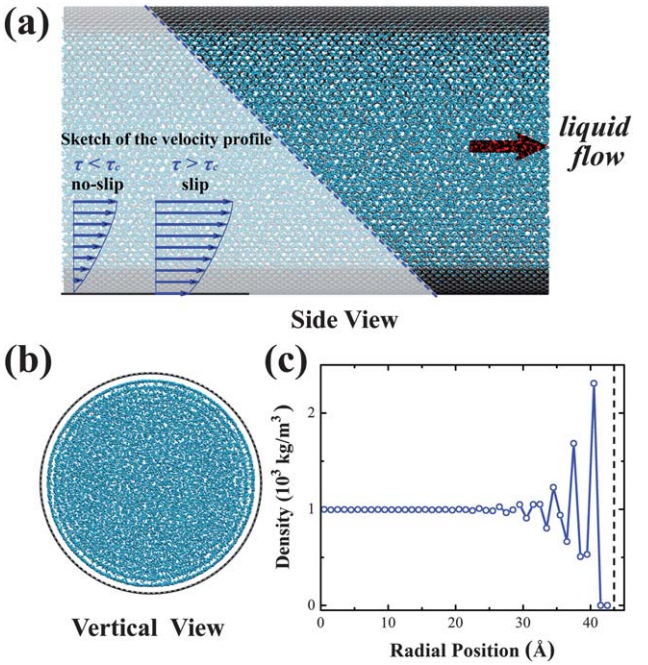

Fig. 1 (a) Side view of the snapshot from our MD simulations and illustration of the critical shear stress. Part of the CNT was cut for clarity. (b) Vertical view of the liquid flow in the CNT. The layered structure of the liquid near the CNT can be found. (c) Radial density profiles of the liquid. The dash line indicates the position of the CNT wall.

represented by simple Lennard-Jones (LJ) particles so that the influence of the intramolecular bond and the Coulomb interactions can be excluded. The average liquid density is 1.0×10^3 kg m^{-3}. The exerted shear stress τ_{ext} and the liquid–solid interaction ε were chosen as the control parameters in our MD simulations.

In our simulations, the liquid–liquid and liquid–solid interactions were described by the standard pairwise LJ potential:

$$E(r) = 4\varepsilon\left[\left(\frac{\sigma}{r}\right)^{12} - \left(\frac{\sigma}{r}\right)^{6}\right], \quad (1)$$

where r is the distance between any pair of atoms. The parameters ε and σ are, in the usual manner, related respectively to the depth of the potential well and the effective molecular diameter. The LJ parameters ε_l and σ_l for liquid–liquid interactions were chosen for $\varepsilon_l = 0.426$ kJ mol^{-1} and $\sigma_l = 3.188$ Å, where the subscript l denotes the liquid. The wetting property of the solid surface, which can be characterized by the contact angle, is a function of ε as well as σ. Thus, the relationship between contact angle behavior and LJ parameters can be established. It has been verified that the contact angle increases as ε decreases.[32] The parameters for liquid–solid interactions were taken as $\varepsilon = N\varepsilon_0$ and $\sigma = 3.19$ Å, where $\varepsilon_0 = 0.392$ kJ mol^{-1} and the subscript 0 indicates that it is a benchmark value. This choice seems somewhat arbitrary but does not affect our results qualitatively. Moreover, it can allow us to set the values systematically according to the value of N. To model the CNT with different wetting properties, various relative liquid–solid interactions were investigated, such as $\varepsilon/\varepsilon_0 = 1$, 5, 10, 15 and 20. The cutoff for these LJ interactions was set to be 10.0 Å.

Simulations were carried out in the NVT ensemble. The equations of motion were solved using a velocity-Verlet algorithm with a time step of 1.0 fs. The system was thermally equilibrated for 1.0 ns using a Nose–Hoover thermostat.[33] The CNT was fixed and only the liquid was thermostated at 298 K. The thermostat was only applied to the directions perpendicular to the flow, to avoid the influence of the thermostating method on the hydrodynamic velocities. Periodic boundary condition was imposed in the flow direction. After the equilibration run, the liquid flow in the CNT was driven by exerting an acceleration a_{ext} to each liquid molecule, as the usual procedure of the simulation of Poiseuille flow in a channel.[16,29,34] The shear stress is $\tau_{ext} = \rho a_{ext} R/2$, in which R is the radius of CNT and ρ is the density of the liquid. All the MD simulations presented in this work were performed using LAMMPS.[35] Since LAMMPS cannot count the average properties along the radial direction, we modified the code to be able to extract the radial profiles of density and velocity. When calculating the radial density profile, as shown in Fig. 1(c), the channel was divided into many thin shells with a uniform thickness along the radial direction. The density of each thin shell was calculated and averaged over a time duration of 5.0 ns. The velocity profile was acquired in a similar way.

We plotted the radial density profile of the liquid flow in the CNT in Fig. 1(c). The strong density oscillations indicate that the liquid presents an ordered structure at the interface, which expends several layers. By contrast, the liquid in the central region of the CNT has a uniform density as the bulk liquid. By comparing the velocity profiles for different shear stresses plotted in Fig. 2, we can see that the transition from the no-slip regime to the slip regime occurs only when a critical shear stress τ_c has to be overcome. When $\tau_{ext} < \tau_c$, the liquid layer adjacent to the CNT inner wall sticks; while $\tau_{ext} > \tau_c$, it starts to slip. Detailed discussions on the critical shear stress and the slip velocity will be presented in the following sections.

3. Theoretical analysis

The Eyring's MKT[31] was introduced to describe the boundary slip at the liquid–solid interface, in which the liquid flow is treated as a rate process.[36,37] Although the inner wall of the CNT is atomically flat, the liquid molecules at the interface are supposed to be in a symmetrical potential energy barrier with the height of E_0. E_0 is also called the activation energy which means the minimum energy required for a liquid molecule jumping from one equilibrium position to the next, as illustrated in Fig. 3. When a shear stress τ is applied to the liquid, the slip velocity is

$$V_s = 2\lambda \frac{k_B T}{h} \frac{F_+}{F_0} \exp\left(-\frac{E_0}{k_B T}\right) \sinh\left(\frac{\tau S \lambda}{2 k_B T}\right), \quad (2)$$

in which T is the absolute temperature, k_B is the Boltzmann constant and h is the Planck constant. F_+ and F_0 are the partition functions for the activated and initial states, respectively. S is the effective area per molecule along the flowing direction. λ is the equilibrium separation, which can characterize the energy corrugation of the solid surface.

The MKT model gives the slip velocity directly, according to eqn (2), and yet there is no description of the critical shear stress τ_c. Attempts to give the theoretical derivation of τ_c inevitably lead to the problem of how to distinguish the slip from the noise and fluctuations in a physical system. Here we proposed a simple comparative analysis of the slip velocity obtained from MKT and the typical fluctuation of thermal velocity, V_f. On the one hand, once the shear stress is imposed, if the so-called slip velocity cannot be discerned from the fluctuation of thermal velocity, there is no slip. That is, such a small shear stress could only enhance the thermal motion of the liquid molecules, rather than induce a steady slip flow. Thus we supposed that the smallest slip velocity should be of the same order as V_f. It is difficult to give the expression of V_f, and we just considered it as a constant for a certain system, which is much smaller than the thermal velocities. On the other hand, the magnitude of the slip velocity when $\tau_{ext} = \tau_c$ can be obtained from eqn (2). The work done by the shear stress (on the order of τ_c) on each liquid molecule, $\tau S \lambda$, is much smaller compared to $k_B T$. Thus the hyperbolic sine function in eqn (2) can be reduced to the linear function. By balancing the two smallest slip velocities, one obtains,

$$\tau_c = V_f \left(\frac{\lambda^2 S}{h} \frac{F_+}{F_0}\right)^{-1} \exp\left(\frac{E_0}{k_B T}\right). \quad (3)$$

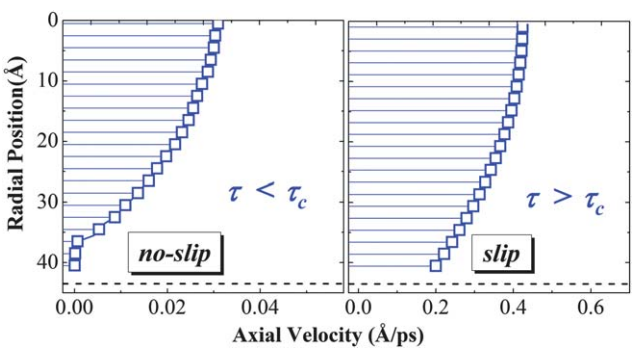

Fig. 2 The radial velocity profiles of the liquid flow under different shear stress. The radial velocity profiles shows that the slip starts only when the shear stress exceeds a critical value τ_c. The dash line indicates the position of the CNT wall.

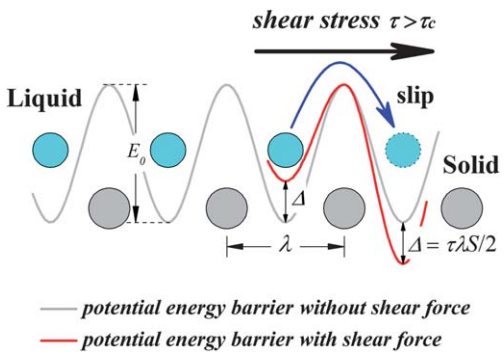

Fig. 3 A sketch of the molecular slip with the approach of MKT. The interfacial liquid molecules in an equilibrium state are located at the bottom of the potential energy barrier (gray curve). When a shear stress larger than τ_c is applied, the height of the potential energy barrier will be changed (red curve) and the liquid molecule can pass over the barrier causing the slip.

Since we have verified that only if the shear stress exceeds τ_c does the slip take place, τ in eqn (2) should be written as $\tau = \tau_{ext} \cdot H[\tau_{ext} - \tau_c]$, in which H[*] is the Heaviside step function.

Given the introduction of critical shear stress, eqn (2) was extended to provide a clear mechanism for boundary slip that the slip starts when the liquid flow overcomes the critical shear stress, which divides the no-slip and slip regimes. Once the slip starts, it should be noted that the slip velocity is affected by various physical parameters,[2] such as the shear rate (or shear stress),[11–15] the wetting properties of the solid surface,[32] the surface curvature,[16] and the surface roughness.[38] If we focus on the shear stress effect, at low shear stress, eqn (2) can be simplified to be

$$V_s = \tau/k, \tag{4}$$

where

$$k = \left(\frac{\lambda^2 S}{h}\frac{F_+}{F_0}\right)^{-1} \exp\left(\frac{E_0}{k_B T}\right). \tag{5}$$

In a sense, k is analogous to the friction coefficient presented in Brillouin's expression. For a Newtonian liquid, $\tau = \eta\dot{\gamma}$, eqn (4) can be written as

$$V_s = \eta\dot{\gamma}/k = L_s\dot{\gamma}, \tag{6}$$

which is equivalent to Navier's SBC.

At high shear stress, the hyperbolic sine can not be simply reduced to a linear function. However, one can still rewrite eqn (2) to be

$$V_s = V_0 \sinh(\tau/\tau_0), \tag{7}$$

where $V_0 = [2\lambda k_B T F_+ /(hF_0)]\exp(-E_0/k_B T)$ is a characteristic velocity and $\tau_0 = 2k_B T/S\lambda$ is a characteristic shear stress. One may find that demarcation between the Navier slip regime and the shear-dependent slip regime is determined by whether the hyperbolic sine expression can be simplified to a linear function for a certain shear stress. Eqn (7) can be used to describe the shear-dependent slip. At even higher shear stress, the slip behavior becomes complicated and the effect of the wetting properties of the solid surface must be considered. We will discuss on this issue in Sec. 4.3.

4. Results and discussion

4.1. The critical shear stress

Our theoretical derivation eqn (3) shows that the critical shear stress is proportional to $\exp(E_0/k_B T)$. Actually, the height of the energy barrier E_0 is connected with the MD parameter ε, which is used to represent the liquid–solid interactions. Since the liquid–solid interactions were modeled by the LJ potential, the maximum and minimum potential energy of the liquid molecule on the solid surface can be calculated. The height of the energy barrier is the difference between the two extrema values. One can obtain a linear relationship $E_0 = C\varepsilon$, in which C is a constant for a certain system. MD results of the dependence of τ_c on the relative liquid–solid interaction $\varepsilon/\varepsilon_0$ were illustrated in Fig. 4. We found that τ_c increases exponentially with ε, which can be well fitted with an exponential function, as the theoretical prediction

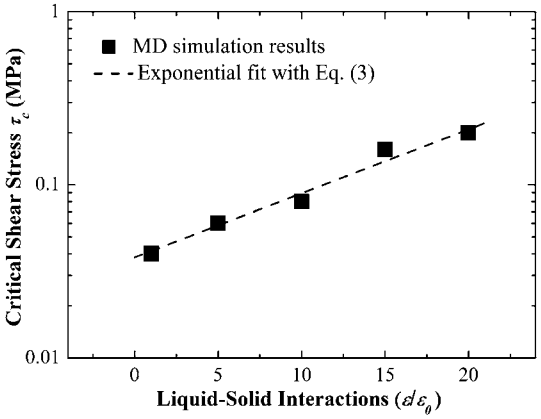

Fig. 4 The quantitative dependence of the critical shear stress on the liquid–solid interactions. The dash line was fitted with an exponential function.

presented in eqn (3). The strong liquid–solid interaction reduces the mobility of the liquid layer adjacent to the solid surface in the tangential direction,[39] thus the critical shear stress increases with the liquid–solid interaction. The values of τ_c reported in our MD simulations are of the order of 0.1 MPa. Generally speaking, this threshold for macroscopic systems is too large to observe the boundary slip. While for micro-, especially nano-channels, the shear stress is enhanced due to the large shear rate, which is estimated with $\tau = \eta\dot{\gamma}$. Thus slip is mostly reported in microscopic experiments. In practice, τ_c depends on the properties of the chosen liquid and solid, which can be described with the surface wettability. We also can see from eqn (3) that the critical shear stress is a function of λ, which can be described as the crystallographic lattice constant of the solid and the temperature T.

4.2. Comparison between MD results and the extended MKT slip model

The slip velocity depends on both the exerted shear stress and wetting properties of the solid surface. In Fig. 5, we presented MD results of the slip velocity as a function of τ_{ext} and ε. The applied shear stress τ_{ext} ranges from τ_c to a maximum value τ_m corresponding to the friction force the CNT can endure. Under low shear stress, the slip velocity increases linearly, which is consistent with the previous studies.[11–13] Under high shear stress, the increase of the slip velocity exhibits two distinct nonlinear responses, which are sensitive to ε. The variation of ε reflects the different wetting properties of the CNT inner wall. For a low ε, the slip velocity increases rapidly with τ_{ext}, until τ_m is reached. Then the liquid would be sped up and the slip velocity increases consistently, which implies the critical shear rate at which the slip length diverges.[11] For this case, our MD results can be well fitted with the theoretical model described in eqn (7). In contrast, a high ε induces a slower increase of the slip velocity. The corresponding slip velocities diverge from the prediction of the extended MKT slip model (Fig. 5). These results indicate that there are some underlying mechanisms for such cases. Martini *et al.* reported similar results, which were attributed to whether the solid wall is fixed or flexible.[14] Since rigid CNT walls were used in our MD simulations, the heat transfer from the liquid to the solid wall is not the only

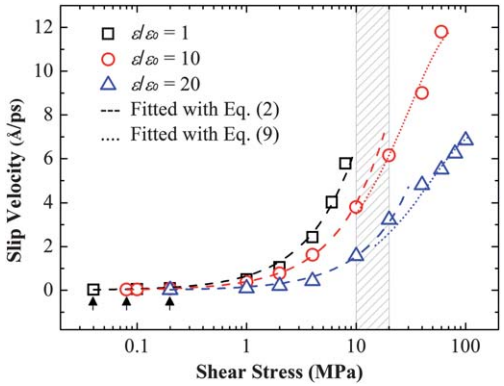

Fig. 5 MD results of the slip velocity as a function of τ_{ext} and ε. Three different types of the liquid–solid interactions ($\varepsilon/\varepsilon_0 = 1$, 10 and 20) were investigated. The MD results were fitted with the SBC proposed in eqn (2) (dash lines). The upward arrows indicate the critical shear stress. Shaded bars are used to represent when the transition from Poiseuille-like to plug-like flow starts. Under high shear stress, MD results were fitted with the extended MKT slip model with a dissipation factor (dot lines). For $\varepsilon/\varepsilon_0 = 1$, the dissipation factor vanishes, since the shear stress exceeded the maximum value τ_m before the transition was observed.

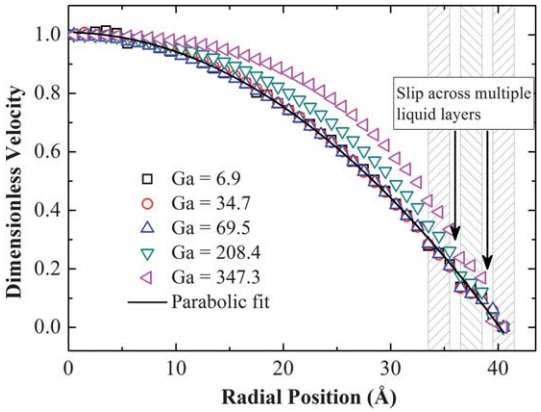

Fig. 6 Dimensionless velocity profiles of various modified Galilei numbers, Ga. The velocity profiles in the middle of the CNT show a transition from Poiseuille-like to plug-like flow as Ga increases. It can be found that the relative sliding between the liquid layers near the interface is remarkable for high Ga. Shaded bars are used to represent the liquid layers at the interface.

route for the energy dissipation at such high shear stress. Detailed discussions are proposed in the following sub-section.

4.3. Energy dissipation at the interface

The MKT can represent the slip behavior well for weak liquid–solid interactions, as well as strong liquid–solid interactions under low shear stress. When considering the latter case under even higher shear stress, the MKT must be modified. As shown in Fig. 1(c), MD simulations indicated that a layering structure of the liquid can be observed at the liquid–solid interface, which is induced by the wall potential. The slip occurs not only at the liquid–solid interface but also within the liquid between the individual layers (Fig. 6). The collective motion of the individual liquid layers has a distinct influence on the flow behavior under high shear stress. In the original framework of the MKT, only friction dissipation due to the energy corrugation of the solid surface was considered. However, the energy dissipation resulting from the relative sliding between the individual liquid layers near the interface must be taken into account. For a force-driven nanotube flow, the work done by the driving force is balanced by the viscous dissipation of the bulk liquid in the middle of the CNT, the energy dissipation due to the slip at the interface,[40] and the energy dissipation contributed from the friction between the liquid layers. The latter two can be expressed in the form of Lord Rayleigh's dissipation function. Consequently, the total rate of the energy conversion is

$$2\pi L a_{ext}\int_0^R \rho(r)V(r)\mathrm{d}r = 2\pi L\int_0^{R-\delta}\eta[\partial V(r)/\partial r]^2 r\mathrm{d}r + k_s V_s^2 + \sum_{i=1}^{n} k_i \Delta V_i^2. \quad (8)$$

In eqn (8), it is assumed that there are n liquid layers near the interface and the total thickness of the liquid layers is δ. V_s is the slip velocity at the interface and k_s is the corresponding friction coefficient. ΔV_i and k_i are the relative velocity and the friction coefficient between the i and $i + 1$ layers. The remarkable relative sliding between the liquid layers at high shear stress results in a significant increase of the friction dissipation near the interface. The corrugation of the potential surface at the interface is determined by not only the liquid–solid interactions, but also the contribution due to the liquid environment.[36] To include the influence of the energy dissipation at high shear stress, we modified eqn (7) to be multiplied by a dissipation factor f_d and obtained

$$V_s = f_d V_0 \sinh(\tau/\tau_0). \quad (9)$$

It should be noted that the friction between the liquid layers at high shear stress is too complicated to describe using a simple explicit expression. Inspired from the studies of the rate dependent friction at the solid interfaces,[41] the dissipation factor is formulated to be proportional to an exponential decay of the shear stress. $f_d = C_1\exp(-C_2\tau)$, in which C_1 and C_2 are the fitting parameters. Eqn (9) is referred to as the extended MKT slip model in this work.

In the low ε cases, the dissipation factor in eqn (9) would vanish, and the corresponding SBC can be simplified to be eqn (7). For the relative liquid–solid interaction $\varepsilon/\varepsilon_0 = 10$ and 20, the introduction of the dissipation factor into the MKT model can represent the slower increase of the slip velocities (shown in Fig. 5).

4.4. Comparison of the extended MKT slip model and other slip models

By introducing the critical shear stress and the dissipation factor, we have proposed a new SBC based on MKT. As discussed in Sec. 3, our model can be used to describe the Navier slip as well as the shear-dependent slip behavior. For the shear-dependent slip, Thompson and Troian has proposed a widely used general SBC,[11] which takes the form of

$$L_s = L_{s0}(1 - \dot{\gamma}/\dot{\gamma}_c)^{-1/2}, \quad (10)$$

where $\dot{\gamma}_c$ is the critical shear rate at which the slip length diverges. The slip length is a power law function of the shear rate, which was observed in MD simulations. By contrast, the extended MKT model has a more distinct physical significance, since it gives a physical picture of the liquid flow near a solid surface. To compare with eqn (10), we changed the extended MKT model to the expression of L_s.

Using $\tau = \eta\dot{\gamma}$ and $V_s = L_s\dot{\gamma}$, eqn (9) can be modified to be

$$L_s = f_d L_{s0} \sinh(\dot{\gamma}/\dot{\gamma}_0'), \tag{11}$$

in which $L_s0 = V_0/\dot{\gamma}$ and $\dot{\gamma}_0' = \tau_0/\eta$. We plotted the results for these two models according to eqn (10) and (11), shown in Fig. 7. Without regard to the dissipation factor, the hyperbolic sine expression of the slip length shows a similar trend as the power law relationship if the appropriate parameters are chosen. When taking into account f_d, the extended MKT slip model exhibits a plateau of the slip length at high shear rate, which is indicated in the variable-density Frenkel-Kontorova (vdFK) model suggested by Lichter *et al.*[12] The observed plateau of the slip length reflects the slower increase of the slip velocity, which is a consequence of the momentum transfer among the bulk liquid and the liquid layers near the interface. Consequently, with the introduction of the appropriate dissipation factor, the extended MKT model combines both features of the two existing models.[11,12]

As expressed in eqn (2), one can notice that the temperature effect of the boundary slip is involved in the MKT model, which can also be compared with previous works.[36]

4.5. Transition from Poiseuille-like to plug-like flow

In Fig. 6, the dimensionless velocity profiles under various shear stresses were plotted. The dimensionless velocity is expressed as $V_{dim} = (V - V_s)/(V_m - V_s)$, in which V_m is the maximum value of the corresponding velocity profile. We can find that: (i) there exists a transition from Poiseuille-like to plug-like flow in the middle of the CNT for strong liquid–solid interactions under much higher shear stress; (ii) near the interface, the slip was observed to be across the multiple liquid layers. They are the two representative features of the nanotube flow which were observed in our MD simulations of high shear stress range. Both of them are closely related to the energy dissipation, which has a significant influence on the boundary slip. The relative sliding between the liquid layers near the wall can be attributed to the slow dynamic processes of the interfacial liquid. The transition of the velocity profiles represents the behavior of the bulk liquid in response to the increasing driven force. The flow behavior in a CNT is codetermined by the external driving force $F_{ext} = a_{ext}\rho\pi R^2 L$ and the intrinsic viscous force of the liquid, which can be written as $F_{vis} = \eta^2/\rho$.[42] A dimensionless number, $Ga = F_{ext}/F_{vis} = a_{ext}\rho^2 R^2 L/\eta^2$, termed as the modified Galilei number in this work, is suggested to compare the relative importance of these two forces. If a pressure-driven flow is considered, it can be written as $Ga = \Delta p\rho R^2/\eta^2$, in which Δp is the pressure drop along the channel. From the data presented in Fig. 6, Ga = 150 can be chosen as a critical value, at which the transition starts. When Ga < 150, the viscous force dominates and the parabolic velocity profiles are in excellent agreement with the Hagen–Poiseuille solutions. When Ga > 150, the driving force dominates and a transition to a plug-like flow was observed. For these results, we have checked the viscosity of the liquid over the whole range of the applied shear stress. The liquid viscosity remains constant for a low driving force, and decreases as the driving force increases. It seems that Ga exceeding the critical value leads to non-Newtonian behavior of the simple liquid. To give a detailed analysis of the influence of Ga on the nano-flow, we are motivated to further explore this issue. The modified Galilei number can also be obtained *via* the dimensional reduction of the governing parameters of this problem, which include: the liquid density ρ, the liquid viscosity η, the external acceleration a_{ext}, the velocity of the liquid V, the CNT radius R and the length L. According to Buckingham's Π-theorem, there are three independent dimensionless numbers: the modified Galilei number $\Pi_1 = Ga = a_{ext}\rho^2 R^2 L/\eta^2$, the well-known Reynolds number $\Pi_2 = Re = \rho VR/\eta$, and the slenderness ratio of the CNT $\Pi_3 = L/R$. The typical Reynolds number in our simulations is very small, *i.e.*, the inertial force is negligible compared to the viscous force. In these cases, the modified Galilei number, rather than the Reynolds number, dominates the liquid transport in the force-driven flow.

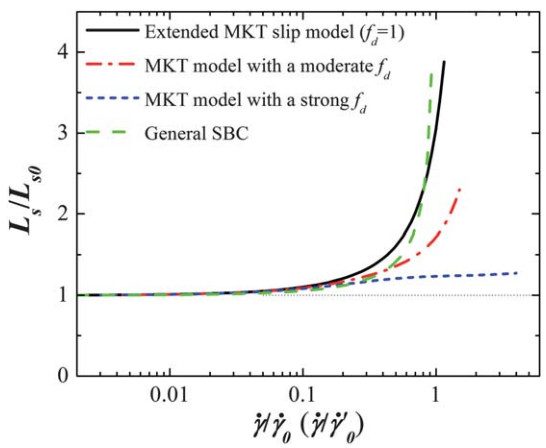

Fig. 7 A comparison of slip length calculated from the extended MKT slip model and other models.

5. Conclusions

In this work, a new SBC is proposed for nanofluidic flow based on Eyring's MKT, which was extended by the introduction of the critical shear stress and the energy dissipation at the liquid–solid interface. Using parameters consistent with the MD simulations, the extended MKT slip model is as stated in eqn (9) and a simplified form is also given in eqn (7). The slip starts when the liquid flow overcomes the critical shear stress, which shows an exponential relationship with the liquid–solid interactions. Considering the energy dissipation resulting from the relative sliding between the liquid layers near the interface, our SBC extends the investigation of the boundary slip to a much high shear stress level, which is in excellent agreement with the MD results. We also suggested a dimensionless modified Galilei number, Ga, to compare the relative importance of the exerted driving force and the intrinsic viscous force of the liquid, which is dominative in the nanoscale force-driven flow. Our new SBC provides a definite expression of the amount of slip and can be used to characterize the slip behavior over a large range of shear

stress, which can be compared with other existing slip models. Besides the driving force and the wetting properties of the solid surface, the slip behavior is sensitive to the surface roughness, thus a two-dimensional MKT-based approach should be explored in the future.

Acknowledgements

This work was jointly supported by the National Basic Research Program of China (973 Program, Grant No. 2007CB310500), the National Natural Science Foundation of China (NSFC, Grant Nos. 60936001 and 11072244) and the Shanghai Supercomputer Center.

References

1 G. K. Batchelor, *An Introduction to Fluid Dynamics*, Cambridge University Press, Cambridge, 1970.
2 E. Lauga, M. P. Brenner and H. A. Stone, in *Handbook of Experimental Fluid Dynamics*, ed. C. Tropea, A. Yarin and J. F. Foss, Springer, New York, 2007.
3 C. Neto, D. R. Evans, E. Bonaccurso, H. J. Butt and V. Craig, *Rep. Prog. Phys.*, 2005, **68**, 2859–2897.
4 O. I. Vinogradova, *Langmuir*, 1995, **11**, 2213–2220.
5 J. Baudry, E. Charlaix, A. Tonck and D. Mazuyer, *Langmuir*, 2001, **17**, 5232–5236.
6 Y. Zhu and S. Granick, *Phys. Rev. Lett.*, 2001, **87**, 096105.
7 V. Craig, C. Neto and D. Williams, *Phys. Rev. Lett.*, 2001, **87**, 054504.
8 E. Bonaccurso, M. Kappl and H. J. Butt, *Phys. Rev. Lett.*, 2002, **88**, 076103.
9 C. Cottin-Bizonne, B. Cross, A. Steinberger and E. Charlaix, *Phys. Rev. Lett.*, 2005, **94**, 056102.
10 O. I. Vinogradova, K. Koynov, A. Best and F. Feuillebois, *Phys. Rev. Lett.*, 2009, **102**, 118302.
11 P. A. Thompson and S. M. Troian, *Nature*, 1997, **389**, 360–362.
12 S. Lichter, A. Roxin and S. Mandre, *Phys. Rev. Lett.*, 2004, **93**, 086001.
13 N. V. Priezjev, *Phys. Rev. E: Stat., Nonlinear, Soft Matter Phys.*, 2007, **75**, 051605.
14 A. Martini, H. Y. Hsu, N. A. Patankar and S. Lichter, *Phys. Rev. Lett.*, 2008, **100**, 206001.
15 A. Niavarani and N. V. Priezjev, *Phys. Rev. E: Stat., Nonlinear, Soft Matter Phys.*, 2010, **81**, 011606.
16 K. Falk, F. Sedlmerier, L. Joly, R. R. Netz and L. Bocquet, *Nano Lett.*, 2010, **10**, 4067–4073.
17 C. L. M. H. Navier, *Mem. Acad. Sci. Inst. Fr.*, 1823, **6**, 389–440.
18 M. Brillouin, *Leçons sur la Viscosité des Liquides et des Gaz*, Gauthier-Villars, Paris, 1907.
19 G. Karniadakis, A. Beskok and N. Aluru, *Microflows and Nanoflows: Fundamentals and Simulation*, Springer, New York, 2005.
20 Q. Z. Yuan and Y. P. Zhao, *J. Am. Chem. Soc.*, 2009, **131**, 6374–6376.
21 P. Xiu, B. Zhou, W. P. Qi, H. J. Lu, Y. S. Tu and H. P. Fang, *J. Am. Chem. Soc.*, 2009, **131**, 2840–2845.
22 S. M. Saparov and P. Pohl, *Proc. Natl. Acad. Sci. U. S. A.*, 2004, **101**, 4805–4809.
23 L. Bocquet and J. L. Barrat, *Soft Matter*, 2007, **3**, 685–693.
24 A. Martini, A. Roxin, R. Q. Snurr, Q. Wang and S. Lichter, *J. Fluid Mech.*, 2008, **600**, 257–269.
25 J. A. Thomas and A. J. H. McGaughey, *Phys. Rev. Lett.*, 2009, **102**, 184502.
26 H. Spikes and S. Granick, *Langmuir*, 2003, **19**, 5065–5071.
27 J. S. Ellis and M. Thompson, *Phys. Chem. Chem. Phys.*, 2004, **6**, 4928–4938.
28 I. Hanasaki and A. Nakatani, *J. Chem. Phys.*, 2006, **124**, 144708.
29 S. Joseph and N. R. Aluru, *Nano Lett.*, 2008, **8**, 452–458.
30 J. A. Thomas and A. J. H. McGaughey, *Nano Lett.*, 2008, **8**, 2788–2793.
31 S. Glasstone, K. J. Laidler and H. Eyring, *The Theory of Rate Processes*, McGraw-Hill, New York, 1941.
32 R. S. Voronov, D. V. Papavassiliou and L. L. Lee, *Ind. Eng. Chem. Res.*, 2008, **47**, 2455–2477.
33 W. G. Hoover, *Phys. Rev. A: At., Mol., Opt. Phys.*, 1985, **31**, 1695–1697.
34 R. Z. Wan, S. Y. Li and H. P. Fang, *Chin. Phys. Lett.*, 2010, **27**, 084702.
35 S. J. Plimpton, *J. Comput. Phys.*, 1995, **117**, 1–19.
36 S. Lichter, A. Martini, R. Q. Snurr and Q. Wang, *Phys. Rev. Lett.*, 2007, **98**, 226001.
37 F. Q. Yang, *Chem. Eng. Commun.*, 2010, **197**, 544–550.
38 E. Bonaccurso, H. J. Butt and V. Craig, *Phys. Rev. Lett.*, 2003, **90**, 144501.
39 Q. Z. Yuan and Y. P. Zhao, *Phys. Rev. Lett.*, 2010, **104**, 246101.
40 T. Z. Qian, X. P. Wang and P. Sheng, *J. Fluid Mech.*, 2006, **564**, 333–360.
41 H. Ullah, M. A. Irfan and V. Prakash, *J. Tribol.*, 2007, **129**, 17–22.
42 E. M. Purcell, *Am. J. Phys.*, 1977, **45**, 3–11.

